Hindawi Publishing Corporation
Journal of Nanomaterials
Volume 2016, Article ID 1497983, 9 pages
http://dx.doi.org/10.1155/2016/1497983

Research Article

Study on Stability and Electrochemical Properties of Nano-$LiMn_{1.9}Ni_{0.1}O_{3.99}S_{0.01}$-Based Li-Ion Batteries with Liquid Electrolyte Containing $LiPF_6$

Monika Bakierska,[1] Michał Świętosławski,[1] Marta Gajewska,[2] Dorota Majda,[1] Marek Drozdek,[1] and Marcin Molenda[1]

[1]*Faculty of Chemistry, Jagiellonian University, Ingardena 3, 30-060 Krakow, Poland*
[2]*Academic Centre for Materials and Nanotechnology, AGH University of Science and Technology, Mickiewicza 30, 30-059 Krakow, Poland*

Correspondence should be addressed to Marcin Molenda; molendam@chemia.uj.edu.pl

Received 13 March 2016; Accepted 23 June 2016

Academic Editor: Ungyu Paik

Herein, we report on the stability and electrochemical properties of nanosized Ni and S doped lithium manganese oxide spinel ($LiMn_{1.9}Ni_{0.1}O_{3.99}S_{0.01}$, LMN1OS) in relation to the most commonly used electrolyte solution containing $LiPF_6$ salt. The influence of electrochemical reaction in the presence of selected electrolyte on the LMN1OS electrode chemistry was examined. The changes in the structure, surface morphology, and composition of the LMN1OS cathode after 30 cycles of galvanostatic charging/discharging were determined. In addition, thermal stability and reactivity of the LMN1OS material towards the electrolyte system were verified. Performed studies revealed that no degradative effects, resulting from the interaction between the spinel electrode and liquid electrolyte, occur during electrochemical cycling. The LMN1OS electrode versus $LiPF_6$-based electrolyte has been indicated as an efficient and electrochemically stable system, exhibiting high capacity, good rate capability, and excellent coulombic efficiency. The improved stability and electrochemical performance of the LMN1OS cathode material originate from the synergetic substitution of $LiMn_2O_4$ spinel with Ni and S.

1. Introduction

The lithium-ion batteries are the most appealing rechargeable energy storage systems in today's consumer electronics market [1–3]. Moreover, due to the high energy and power density, as well as the excellent reversibility and cyclability, Li-ion technology shows great promise in the development of a wide variety of large-scale applications (e.g., hybrid electric vehicles, electric vehicles, and smart grids) [4–6]. However, to face challenges of the more strict energy and environmental policies, it is now essential to further improve these energy storage devices. Therefore, the research in the field of the materials that form lithium-ion batteries and influence their characteristics in terms of electrochemical performance, safety issues, cost, and environmental impact has aroused significant interest.

Layered lithium cobalt oxide ($LiCoO_2$, LCO), lithium nickel oxide ($LiNiO_2$, LNO), and related systems have been commonly used as cathode materials in commercial Li-ion batteries. Nevertheless, with increasing concerns about the availability, high cost, and toxicity of cobalt and nickel based cathodes, the lithium manganese oxide spinel ($LiMn_2O_4$, LMO) is considered to be a favorable candidate. Apart from the abundant resources, low production cost, and environmental benignity, LMO material offers other advantages, such as high working potential, high thermal stability, excellent safety, and competitive theoretical capacity (148 mAh g^{-1}) [7–9]. Unfortunately, stoichiometric spinel exhibits considerable capacity decay during charge-discharge cycling processes which hinders its wide practical use [10, 11]. The reasons for the capacity loss can be particularly attributed to the Jahn-Teller distortion occurring within the crystal structure of the

spinel and manganese dissolution into the electrolyte via the disproportionation reaction ($2Mn^{3+} \rightarrow Mn^{4+} + Mn^{2+}$) [12, 13]. In order to overcome the aforementioned obstacles, many efforts have been made so far and through the most widely adopted methods are element substitution in the spinel structure, surface modification, minimizing the particles size, and optimization of the LMO morphology [14–25].

Among the various substitution strategies, an interesting attempt, which has been recently reported to address the problems of stoichiometric LMO material, is the combined (cation and anion) doping with nickel and sulphur [26, 27]. It has been shown that introduction of Ni and S improves the structural characteristics of the LMO, increasing its cycling ability in Li-ion batteries. However, the possible reaction of the cathode surface with the liquid electrolyte at the high operating voltage, which may lead to decomposition of the electrolyte and cell degradation, is one of the major challenges for the electrochemical stability of LMO-based electrode [28].

As already mentioned, the surface chemistry of lithium manganese oxide spinel and its derivatives is of great importance to the proper operation of Li-ion batteries. Hence, understanding the relations between the electrode performance and the electrolyte composition is crucial [29–31]. Present lithium batteries use mainly organic electrolytes that generally consist of a suitable lithium salt (e.g., $LiPF_6$, $LiClO_4$, $LiBF_4$, and $LiAsF_6$) and one or more solvents. Combinations of alkyl carbonates (e.g., EC, DEC, DMC, and EMC) are the most frequently employed [32, 33]. The formulation of the electrolyte requires the fulfillment of basic specification comprising acceptable conductivity, wide electrochemical window, the ability to form stable solid-electrolyte interface (SEI) layer on electrodes, and broad temperature range of operation [34]. All things considered, it is asserted that the choice of the suitable electrolyte for LMO compound may have a notable impact on the chemical stability and electrochemical characteristics of the Li-ion batteries.

This paper describes our research on the stability and electrochemical properties of $LiMn_{1.9}Ni_{0.1}O_{3.99}S_{0.01}$ (LMN1OS) electrode in contact with the predominant non-aqueous electrolyte for commercial Li-ion cells, a solution of lithium hexafluorophosphate ($LiPF_6$) salt in mixed alkyl carbonates including ethylene carbonate (EC) and diethyl carbonate (DEC). The choice of the electrolyte system was based on the fact that $LiPF_6$ salt together with carbonate solvents demonstrates the best balance of indispensable properties necessary for Li-ion electrolytes, having one of the highest conductivity values and forming a stable interface with aluminium current collector.

2. Materials and Methods

Nanosized Ni and S doped $LiMn_2O_4$ spinel material ($LiMn_{1.9}Ni_{0.1}O_{3.99}S_{0.01}$, LMN1OS) was synthesized by a modified sol-gel method analogously to the procedure for preparing the sulphided spinels which was described in our previous publication [35–37]. The synthesis was carried out under constant flow of argon using aqueous solutions of $CH_3COOLi{\cdot}2H_2O$, $(CH_3COO)_2Mn{\cdot}4H_2O$, $(CH_3COO)_2Ni{\cdot}4H_2O$, $(NH_4)_2S$, and $NH_3{\cdot}H_2O$ in the role of the alkalizing agent. After condensation process, the powder precursor was calcined in air atmosphere at 300°C for 24 h and then at 650°C for 6 h. The heating rates for the thermal treatments were 1°C min^{-1} and 5°C min^{-1}, respectively.

The resulting LMN1OS powder sample, prepared at a calcination temperature of 650°C, was observed under a transmission electron microscopy (TEM) using FEI TECNAI TF20 X-TWIN high-resolution microscope operating at 200 kV.

To check the thermal stability and reactivity of the LMN1OS spinel towards the electrolyte solution, differential scanning calorimetry (DSC) analysis was performed. About 15 mg of active cathode material was placed in aluminium pan and wetted with a few drops of the electrolyte solution. In addition, the pure electrolyte solution was studied to determine the effects related to its thermal decomposition. Both measurements were done using 821^e Mettler-Toledo equipment in the temperature range from 25 to 400°C with a heating rate of 10°C min^{-1} and under constant argon flow.

The electrolyte solution was prepared in an argon-filled glove box (MBRAUN UNIlab workstation with O_2 and H_2O levels less than 0.1 ppm). To obtain 1 M electrolyte system, appropriate amount of $LiPF_6$ salt was dissolved in organic solvents mixture containing the high permittivity EC and low viscosity DEC at a volume ratio of 1 : 1.

In order to determine the stability and electrochemical characteristics of the as-prepared LMN1OS powder during cycling performance, the electrodes were fabricated. The cathodes were prepared by mixing 80 wt.% of active material (LMN1OS), 10 wt.% of carbon black (CB), and 10 wt.% of polyvinylidene fluoride (PVDF) in N-methyl-2-pyrrolidone (NMP). The slurry was then spread onto Al foil and dried in air at 90°C for about 24 h. To form the working electrodes, the cathode foil was cut into circular discs with 12 mm in diameter and pressed so as to enhance the contact between the Al substrate, active material, and conductive carbon additive. Subsequently, the cathode discs were assembled into two-electrode coin-type cell (R2032) using lithium foil as an anode. The electrodes were separated by a microporous Celgard 2325 polypropylene membrane and Whatman GF/F glass microfiber filters. The assembly process of Li/Li^+/LMN1OS cells was carried out in Ar-filled glove box.

To examine the electrochemical behavior of LMN1OS spinel cathode material in the presence of selected electrolyte composition (solution of $LiPF_6$ in EC : DEC), the galvanostatic charge-discharge tests (CELL TEST) were performed on an ATLAS 0961 MBI multichannel battery tester. The cell was cycled between 3.5 and 4.8 V at different current rates at room temperature. The long-term cycling performance of the Li/Li^+/LMN1OS cell was also evaluated. Before the electrochemical measurements, the batteries were aged for about 24 h.

The electrochemical properties of the Li/Li^+/LMN1OS cells before the cycling and after each 10 cycles were characterized by the electrochemical impedance spectroscopy (EIS) studies. The EIS measurements were run at 3.75 V in the frequency range between 100 kHz and 0.1 Hz on a potentiostat/galvanostat Autolab PGSTAT302N/FRA2. The

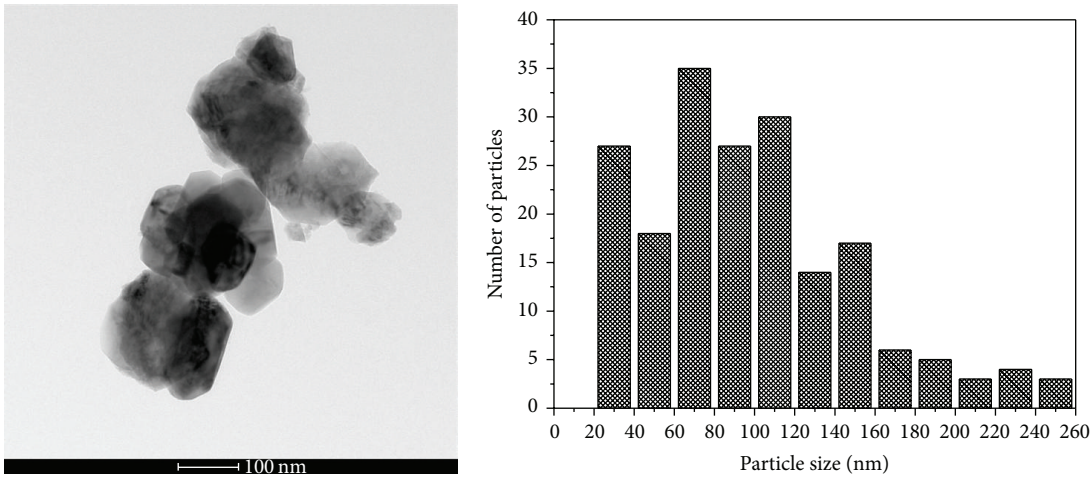

(a) (b)

Figure 1: TEM image of LMN1OS nanoparticles (a) and corresponding histogram (b).

applying amplitude was 0.01 V. The analysis of the EIS data was provided by fitting the experimental data with equivalent circuits, based on the Boukamp model using Nova 1.11 Autolab software.

The changes occurring in the structure, surface morphology, and composition of the LMN1OS electrode after 30 cycles were investigated. To test the cathodes after electrochemical performance, the lithium cell was disassembled and the spinel-based electrode was taken out. To remove the residual electrolyte, the cycled cathode was gently rinsed with DEC.

The crystal structure of the fresh (not exposed to electrolyte) and cycled LMN1OS electrode was identified by powder X-ray diffraction (XRD) using Bruker D2 PHASER diffractometer with Cu Kα radiation (λ = 0.154184 nm). The diffraction data was collected between 10 and 80° (2θ) at a step of 0.02°. To identify the phase composition of the cathodes, structural data from the International Centre for Diffraction Data (ICDD) and American Mineralogist Crystal Structure Database (AMCSD) was used. The average crystallite size of the samples was calculated using Scherrer's formula, taking into account the integral width of (111) reflection of the cubic spinel.

To evaluate the morphology of the spinel-based cathode before and after the electrochemical cycling, an FEI Versa 3D (FEG) scanning electron microscope (SEM) was used.

X-ray photoelectron spectroscopy (XPS) measurements were carried out under ultrahigh vacuum to detect the surface composition of the fresh and cycled electrodes. For this purpose, a Prevac photoelectron spectrometer equipped with a hemispherical VG SCIENTA R3000 analyzer using a focused monochromatized Al Kα radiation ($h\nu$ = 1486.6 eV) was employed. The obtained spectra were fitted using CasaXPS processing software.

3. Results and Discussion

Figure 1(a) presents the TEM image of the prepared Ni and S doped lithium manganese oxide spinel. As it can be seen, the LMN1OS material exhibits high degree of crystallinity. Slight agglomeration among the particles seems to be present in certain regions of the sample. Additionally, based on the microscopy analysis, semispherical shape of the particles with sharp and distinct edges was revealed and nanosized character of the sample was confirmed. The particles size evaluated from TEM observations ranges approximately between 22 and 258 nm with the mean size of about 98 nm. The histogram of particle size distribution, elaborated from consideration of two hundreds of particles, is shown in Figure 1(b).

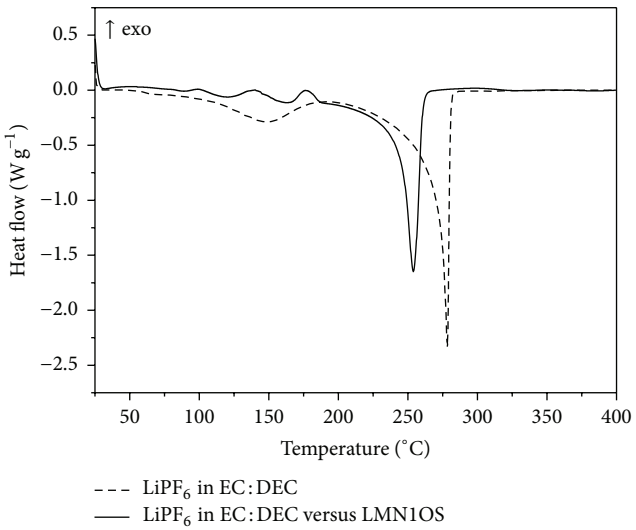

Figure 2: Differential scanning calorimetry of LiPF$_6$ in EC : DEC along with the analysis of its thermal stability towards LMN1OS cathode material.

The thermal and chemical stability of LMN1OS spinel in contact with the chosen electrolyte was established. The results of thermal decomposition of LiPF$_6$ in EC : DEC electrolyte solution are presented in Figure 2 (dashed line). The heat flow curve of the electrolyte system displays several

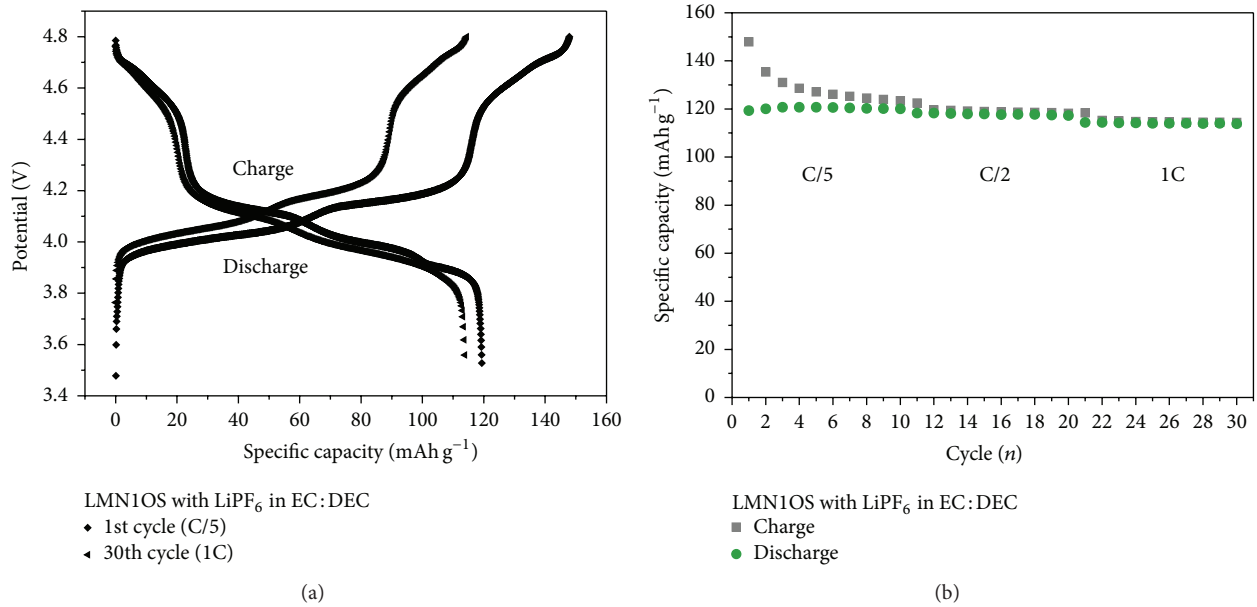

Figure 3: The charge-discharge voltage profiles for the 1st cycle and 30th cycle (a) and rate performance of LMN1OS cathode material (b).

endothermic peaks. The two major effects at around 150 and 275°C are observed for the electrolyte due to the solvents evaporation (DEC and EC, resp.) [33, 38]. Another effect at about 75°C, expressed by a peak of significantly lower heat flow, can be ascribed to the formation of phosphorus oxyfluoride from the reaction of $LiPF_6$ with trace amounts of water [39]. In fact, all the endothermic effects seen upon scanning may also indicate the decomposition of $LiPF_6$ salt as it has an endothermic nature and therefore its response may overlap with other signals [39, 40]. It is also worth noticing that no exothermic peaks over the entire temperature range were perceived. Analogous DSC curve was recorded for electrolyte solution in relation to the LMN1OS cathode material and demonstrated in Figure 2 as well (solid line). As shown, the contact of electrolyte with the electrode active material does not imply any considerable changes in the DSC profile. Nonetheless, slight shift of the onset temperatures of the electrolyte decomposition process and the decrease in the heat values should be noted. This effect is connected with high development of LMN1OS nanopowder surface. Taking the above into account, we maintain that $LiPF_6$ in EC : DEC is the optimal electrolyte system in terms of thermal and chemical stability towards cathode material based on lithium manganese spinel.

To elucidate the influence of electrolyte composition on the operation of Li/Li$^+$/LMN1OS cells, the electrochemical cycling tests using different current densities were conducted at room temperature (the electrode with high active material loading of 1.82 mg cm^{-2} was used). The galvanostatic voltage profiles for the 1st cycle and the 30th cycle at the current rate of C/5 and 1C, respectively, are illustrated in Figure 3(a). The potential curves disclose two regions of electrochemical activity of the LMN1OS sample. This behavior is associated with the four-stage lithium ions intercalation/deintercalation process arising from the oxidation/reduction of manganese (the two major plateaus at ~4.1 V) and nickel (the two minor plateaus at ~4.7 V). The specific charge/discharge capacities achieved at C/5, C/2, and 1C current rates as a function of cycle number can be viewed in Figure 3(b). For the studied cell, the initial charge and discharge capacities reach 147.8 and 119.4 mAh g^{-1}, which gives irreversible charge capacity of about 24%. This irreversible charge originates from the reduction of the electrolyte and formation of the SEI layer. After formation of SEI layer upon first 10 cycles the irreversible capacity decreases and coulombic efficiency of charging/discharging process reaches up to 99.6%. As expected, along with the current rate rise, the discharge capacities decrease to 118.3 (C/2) and 114.4 mAh g^{-1} (1C). In general, the capacity of $LiMn_{1.9}Ni_{0.1}O_{3.99}S_{0.01}$ in comparison to $LiMn_2O_4$ material is moderately deteriorated which can be explained by reduction of the Mn^{3+}/Mn^{4+} redox pair resulting from Ni doping. On the whole, the Li/Li$^+$/LMN1OS cell containing $LiPF_6$ in EC : DEC electrolyte exhibits good rate performance, remaining stable during charging/discharging processes.

The preliminary studies regarding the stability of the LMN1OS cathode material involving differential scanning calorimetry and charge/discharge cycling tests revealed that the employed liquid electrolyte does not affect unfavorably the characteristics of the spinel material and, what is more, the performance of LMN1OS-based Li-ion battery. However, to further verify these outcomes, structure, surface morphology, and composition as well as impedance of the LMN1OS electrode before and after cycling were analyzed.

To further analyze the electrochemical properties of the $LiMn_{1.9}Ni_{0.1}O_{3.99}S_{0.01}$-based Li-ion cell, EIS measurements were run. Figure 4(a) presents Nyquist plots obtained for the Li/Li$^+$/LMN1OS cell before galvanostatic cycling and after each set of 10 cycles at the potential of 3.75 V, at

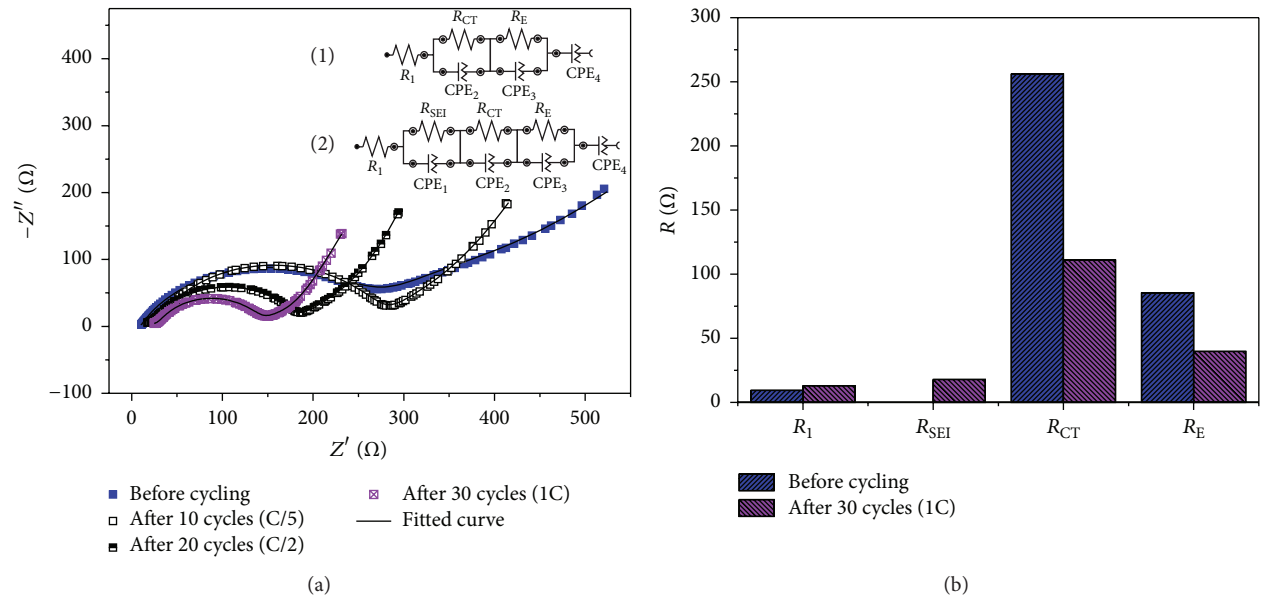

Figure 4: Nyquist plots of the impedance data obtained for Li/Li$^+$/LMN1OS cell (a) and the changes of EIS parameters (b).

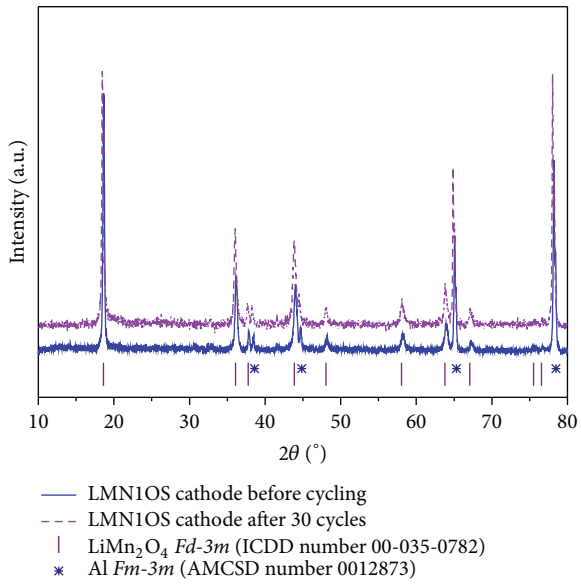

Figure 5: X-ray diffraction patterns of LMN1OS electrode before and after electrochemical cycling tests.

Table 1: Calculated values of resistors from the proposed equivalent circuits for Li/Li$^+$/LMN1OS cell.

	R_1 [Ω]	R_{SEI} [Ω]	R_{CT} [Ω]	R_E [Ω]
Before cycling	9	—	256	86
After 10 cycles (C/5)	12	19	247	86
After 20 cycles (C/2)	10	18	154	86
After 30 cycles (1C)	13	18	111	40

room temperature. The spectrum of the freshly assembled cell (not exposed to the electrolyte) is composed of two depressed semicircles in the high-to-low frequency region and the tail line at the low frequencies. For the cycled cell, another semicircle can be perceived at the high frequencies (representing formation of passivation layer on the material's surface). The equivalent circuits, displayed in the inset of Figure 4(a), were used to model the EIS data. The fitting results are represented in the impedance spectra by the solid lines. In these circuits, R_1 is attributed to the ohmic resistance (the combined resistance of the electrolyte system and contacts of the cell). The first parallel connection of R_{SEI} and CPE_1 elements corresponds to the SEI interphase, while the second combination of common elements (R_{CT} and CPE_2) is ascribed to the charge transfer process. The third parallel join of R_E and CPE_3 elements refers to the electronic properties of the studied spinel cathode material [41]. The last element, linked in series, in the proposed circuits (CPE_4) is responsible for the diffusion of Li$^+$. The values of resistors, estimated from the fit of the impedance data, are gathered in Table 1 and partially demonstrated in Figure 4(b). One can easily see that considerable decrease of R_{CT} and R_E values occurs along with the charging/discharging processes. By contrast, R_1 and R_{SEI} values remain at the same level during electrochemical cycling. This data indicates that LMN1OS electrode versus $LiPF_6$ in EC : DEC electrolyte is an efficient and electrochemically stable system.

The X-ray diffraction patterns of the LMN1OS electrode before and after cycling are displayed in Figure 5. It can be found that XRD pattern of the electrode cycled in the electrolyte does not differ substantially from the pattern of the fresh electrode, having nearly identical peaks intensity. Furthermore, in both cases, the same diffraction peaks, which exactly match the reference patterns of the cubic $LiMn_2O_4$ spinel structure with *Fd-3m* space group (ICDD number 00-035-0782) and aluminium of the cubic structure with *Fm-3m*

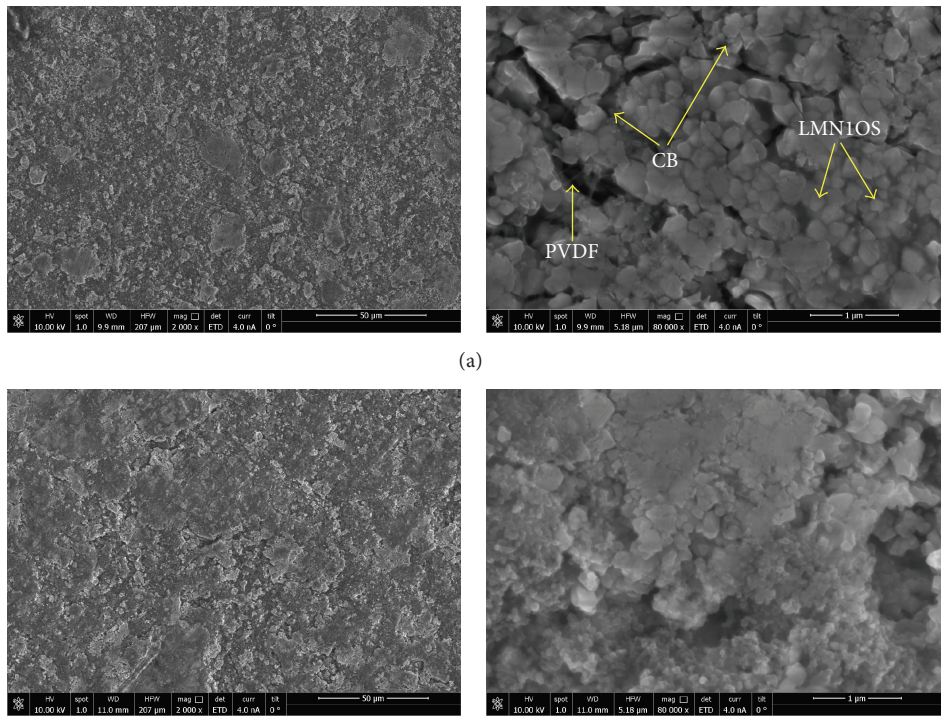

Figure 6: SEM micrographs of the fresh (a) and cycled (b) LMN1OS electrode.

space group (AMCSD number 0012873), are visible. At this point, it should be recalled that Al foil was used as the current collector to fabricate the LMN1OS cathode. No impurity phases were detected. As for the peak positions of XRD profiles, close observation reveals that all the peaks for the cathode after cycling are slightly shifted towards lower values of the diffraction angle (2θ). In addition, the enlargement of lattice constant for the Ni and S doped LMO spinel after the electrochemical reaction was disclosed. The lattice parameters for the fresh electrode and the electrode cycled in the electrolyte are 0.8239 and 0.8312 nm, respectively. The larger lattice constant for the cycled electrode may derive from stretching tensions occurring in the structure during insertion/deinsertion of lithium ions. Even though the electrochemical cycling appears to influence the crystal structure of the spinel, the structure of LMO-based electrode seems to be fairly stable, without apparent deformations. The average crystallite size of the LMN1OS material, calculated for both electrodes using Scherrer's formula, is around 32 nm. The XRD results for the particle size demonstrated evident difference regarding the values found by TEM. The size determined from the XRD is significantly smaller than the particles size estimated based on TEM observations. The point is that the width of the XRD reflection provides information about the average size of the single crystalline domain inside the nanocrystal, whereas TEM images show the total size of a nanoparticle [42].

The morphology of the LMN1OS cathode before electrochemical cycling and after 30 cycles of charging/discharging was investigated using SEM. The representative micrographs are illustrated in Figure 6. The individual components that constitute the electrodes (LMN1OS, active material, CB, conductive agent, and PVDF, binder) are marked in Figure 6(a); however, the same elements can be seen in the remaining SEM image as well (Figure 6(b)). It is worth noticing that the mentioned constituents are quite uniformly distributed over the electrode surface in both states (before and after cycling). As shown, the particles of LMN1OS active material have isotropic, semispherical shape, a smooth surface, and relatively homogeneous size distribution, which is in good accordance with the TEM observations of LMN1OS powder. Observably, the particles morphology of the electrode cycled in the $LiPF_6$ in EC : DEC electrolyte is similar to that of the fresh electrode. As a matter of fact, after the electrochemical reaction, the particle size and shape do not change, suggesting that the electrolyte composition has no effect on the surface morphology of the spinel-based electrode. Besides, no cracks, holes, or separate phases were distinguished in the surface of the cycled electrode. Altogether, the stability of the LMN1OS electrode morphology with regard to the used electrolyte was confirmed.

XPS spectra of LMN1OS electrodes before and after galvanostatic studies (after 30 charge/discharge cycles) were analyzed to observe changes in surface chemistry of the electrodes which occur during electrochemical reaction. Figure 7 presents photoelectron spectra of Mn 2p, O 1s, and C 1s ((a) before and (b) after the electrochemical reaction). Nickel in the spinel structure cannot be analyzed due to the overlapping of signal from Ni 2p photoelectrons with manganese Auger electrons. As regards sulphur, due to its small amount in the spinel structure, the S 2p photoelectron signal is beyond the

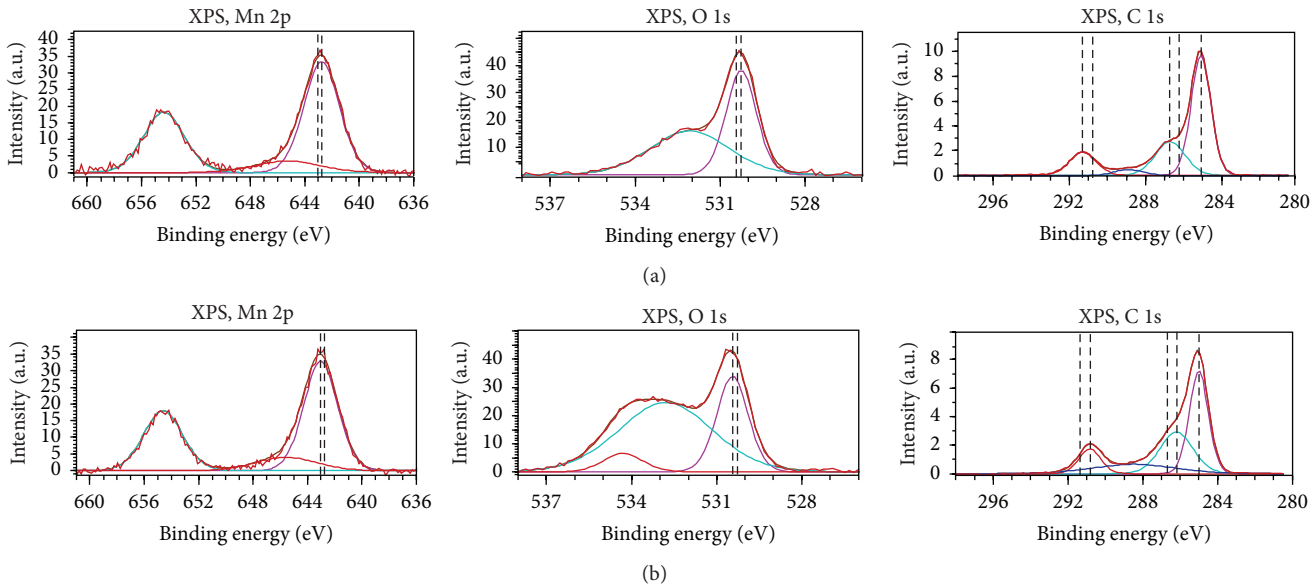

FIGURE 7: The Mn 2p, O 1s, and C 1s XPS spectra of LMN1OS electrode before (a) and after (b) electrochemical reaction.

detection range. Intensities of studied XPS signals from both cases are at the same level which assure lack of contamination or decomposition of the electrode during electrochemical cycling and allow us to fully compare obtained results. As it can be seen in Figure 7, the Mn 2p signal does not change much after 30 consecutive charging/discharging cycles. Slight rise of average oxidation state of manganese can be noticed after electrochemical reaction (minimal shift of Mn $2p_{3/2}$ peak towards higher binding energy) but it is clear that there are no other manganese rich phases or Mn loss from the structure. All of these confirm good structural stability of LMN1OS versus $LiPF_6$-based electrolyte. Both O 1s and C 1s spectra vary after galvanostatic studies. This is connected with passivation of the active material during initial charging/discharging cycles. Passivation is the result of carbonates decay on the electrode surface. Products of this decomposition are located on the material's surface and affect the shape of XPS spectra: shift of the peak observed at 291.3 eV to 290.8 eV (carbonyl groups) and rise of the share of peak at ~288.8 eV (carbonate groups). These results are consistent with EIS studies.

Finally, to check the cycling stability of LMO spinel substituted with Ni and S, referring to the stability of the electrode material towards $LiPF_6$ in EC : DEC electrolyte solution, the Li/Li^+/LMN1OS cell was subjected to the additional long-term galvanostatic tests. In this study, electrode with optimal active material loading of 0.73 mg cm^{-2} was used in the cell which was consecutively charged/discharged at 2C current rate. Figure 8 illustrates the discharge capacities of LMN1OS cathode over 100 cycles. The initial discharge capacity of the sample is 139.5 mAh g^{-1} and declines to 127.2 mAh g^{-1} after 100 cycles. Thereby, the retained discharge capacity for LMN1OS electrode is 91.2%. Apart from the cycling stability, Figure 8 indicates coulombic efficiency which ranges from 97.4% to 99.8%.

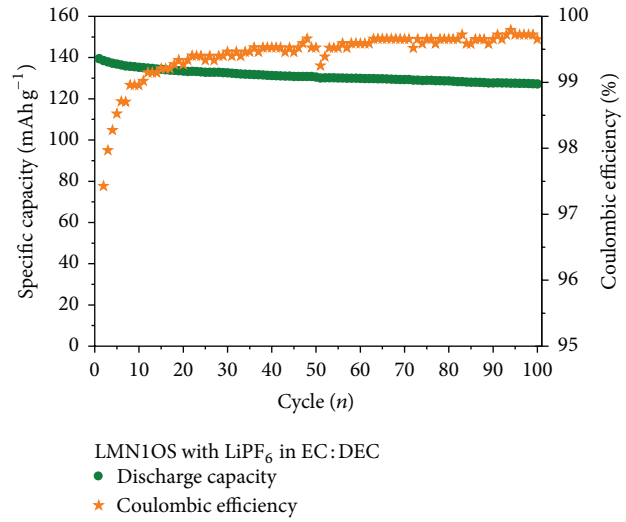

FIGURE 8: The long-term cycling performance of LMN1OS electrode at 2C rate.

4. Conclusions

Study on stability and electrochemical properties of LMN1OS electrode with regard to $LiPF_6$ in EC : DEC electrolyte has been successfully performed. Nanosized character of the Ni and S doped LMO spinel, synthesized by the sol-gel method, was confirmed. The investigations of thermal and chemical stability of LMN1OS spinel using differential scanning calorimetry confirmed accurateness of the electrolyte choice. Moreover, the preliminary charge/discharge cycling tests revealed that the employed liquid electrolyte does not affect unfavorably the electrochemical characteristics of LMN1OS-based Li-ion battery. The structure, surface morphology, and composition of the LMN1OS cathode after galvanostatic

charging/discharging were also found to be stable and not susceptible to interact with the electrolyte. No degradative effects were observed after the electrochemical reaction. Additionally, the formation of a stable passivation layer which ensures high coulombic efficiency (reaching up to 99.8%) and capacity retention was demonstrated. The LMN1OS spinel material can provide stable reversible capacity of approximately 127 mAh g^{-1} (under 2C rate). The loss of initial capacity for LMN1OS sample was only around 9% after 100 cycles at room temperature. Taking all into consideration, it can be pointed out that the improved stability and electrochemical performance of the LMN1OS cathode material arise from the introduction of nickel and sulphur into the LMO spinel structure.

Competing Interests

The authors declare that they have no competing interests.

References

[1] J.-M. Tarascon and M. Armand, "Issues and challenges facing rechargeable lithium batteries," *Nature*, vol. 414, no. 6861, pp. 359–367, 2001.

[2] M. S. Whittingham, "Lithium batteries and cathode materials," *Chemical Reviews*, vol. 104, no. 10, pp. 4271–4301, 2004.

[3] J. B. Goodenough and K.-S. Park, "The Li-ion rechargeable battery: a perspective," *Journal of the American Chemical Society*, vol. 135, no. 4, pp. 1167–1176, 2013.

[4] P. V. Braun, J. Cho, J. H. Pikul, W. P. King, and H. Zhang, "High power rechargeable batteries," *Current Opinion in Solid State and Materials Science*, vol. 16, no. 4, pp. 186–198, 2012.

[5] V. Etacheri, R. Marom, R. Elazari, G. Salitra, and D. Aurbach, "Challenges in the development of advanced Li-ion batteries: a review," *Energy and Environmental Science*, vol. 4, no. 9, pp. 3243–3262, 2011.

[6] M. Hu, X. Pang, and Z. Zhou, "Review Recent progress in high-voltage lithium ion batteries," *Journal of Power Sources*, vol. 237, pp. 229–242, 2013.

[7] K. Amine, J. Liu, I. Belharouak et al., "Advanced cathode materials for high-power applications," *Journal of Power Sources*, vol. 146, no. 1-2, pp. 111–115, 2005.

[8] J. W. Fergus, "Recent developments in cathode materials for lithium ion batteries," *Journal of Power Sources*, vol. 195, no. 4, pp. 939–954, 2010.

[9] C. M. Julien, A. Mauger, K. Zaghib, and H. Groult, "Comparative issues of cathode materials for li-ion batteries," *Inorganics*, vol. 2, no. 1, pp. 132–154, 2014.

[10] E. Iwata, K.-I. Takahashi, K. Maeda, and T. Mouri, "Capacity failure on cycling or storage of lithium-ion batteries with Li–Mn–O ternary phases having spinel-framework structure and its possible solution," *Journal of Power Sources*, vol. 81-82, pp. 430–433, 1999.

[11] L. Yang, M. Takahashi, and B. Wang, "A study on capacity fading of lithium-ion battery with manganese spinel positive electrode during cycling," *Electrochimica Acta*, vol. 51, no. 16, pp. 3228–3234, 2006.

[12] G. Li, Y. Iijima, Y. Kudo, and H. Azuma, "Structural changes of manganese spinel at elevated temperatures," *Solid State Ionics*, vol. 146, no. 1-2, pp. 55–63, 2002.

[13] L.-F. Wang, C.-C. Ou, K. A. Striebel, and J.-S. Chen, "Study of Mn dissolution from $LiMn_2O_4$ spinel electrodes using rotating ring-disk collection experiments," *Journal of the Electrochemical Society*, vol. 150, no. 7, pp. A905–A911, 2003.

[14] Y. Xu, G. Chen, E. Fu et al., "Nickel substituted $LiMn_2O_4$ cathode with durable high-rate capability for Li-ion batteries," *RSC Advances*, vol. 3, no. 40, pp. 18441–18445, 2013.

[15] D.-W. Han, W.-H. Ryu, W.-K. Kim, J.-Y. Eom, and H.-S. Kwon, "Effects of Li and Cl codoping on the electrochemical performance and structural stability of $LiMn_2O_4$ cathode materials for hybrid electric vehicle applications," *Journal of Physical Chemistry C*, vol. 117, no. 10, pp. 4913–4919, 2013.

[16] Y. Fu, H. Jiang, Y. Hu, Y. Dai, L. Zhang, and C. Li, "Synergistic enhancement effect of Al doping and highly active facets of $LiMn_2O_4$ cathode materials for lithium-ion batteries," *Industrial and Engineering Chemistry Research*, vol. 54, no. 15, pp. 3800–3805, 2015.

[17] Z.-J. Zhang, S.-L. Chou, Q.-F. Gu et al., "Enhancing the high rate capability and cycling stability of $LiMn_2O_4$ by coating of solid-state electrolyte $LiNbO_3$," *ACS Applied Materials and Interfaces*, vol. 6, no. 24, pp. 22155–22165, 2014.

[18] Y. Shang, X. Lin, X. Lu, T. Huang, and A. Yu, "Nano-TiO_2(B) coated $LiMn_2O_4$ as cathode materials for lithium-ion batteries at elevated temperatures," *Electrochimica Acta*, vol. 156, pp. 121–126, 2015.

[19] G. H. Waller, P. D. Brooke, B. H. Rainwater et al., "Structure and surface chemistry of Al_2O_3 coated $LiMn_2O_4$ nanostructured electrodes with improved lifetime," *Journal of Power Sources*, vol. 306, pp. 162–170, 2016.

[20] H. Xia, Z. Luo, and J. Xie, "Nanostructured $LiMn_2O_4$ and their composites as high-performance cathodes for lithium-ion batteries," *Progress in Natural Science: Materials International*, vol. 22, no. 6, pp. 572–584, 2012.

[21] Y. Cai, Y. Huang, X. Wang et al., "Facile synthesis of $LiMn_2O_4$ octahedral nanoparticles as cathode materials for high capacity lithium ion batteries with long cycle life," *Journal of Power Sources*, vol. 278, pp. 574–581, 2015.

[22] X. Gao, Y. Sha, Q. Lin, R. Cai, M. O. Tade, and Z. Shao, "Combustion-derived nanocrystalline $LiMn_2O_4$ as a promising cathode material for lithium-ion batteries," *Journal of Power Sources*, vol. 275, pp. 38–44, 2015.

[23] L. Su, Y. Jing, and Z. Zhou, "Li ion battery materials with core-shell nanostructures," *Nanoscale*, vol. 3, no. 10, pp. 3967–3983, 2011.

[24] W. Sun, H. Liu, T. Peng et al., "Hierarchical donut-shaped $LiMn_2O_4$ as an advanced cathode material for lithium-ion batteries with excellent rate capability and long cycle life," *Journal of Materials Chemistry A*, vol. 3, no. 15, pp. 8165–8170, 2015.

[25] H. Zhao, F. Li, X. Liu et al., "A simple, low-cost and eco-friendly approach to synthesize single-crystalline $LiMn_2O_4$ nanorods with high electrochemical performance for lithium-ion batteries," *Electrochimica Acta*, vol. 166, Article ID 24566, pp. 124–133, 2015.

[26] Y. K. Sun, S. W. Oh, C. S. Yoon, H. J. Bang, and J. Prakash, "Effect of sulfur and nickel doping on morphology and electrochemical performance of $LiNi_{0.5}Mn_{1.5}O_{4-x}S_x$ spinel material in 3-V region," *Journal of Power Sources*, vol. 161, no. 1, pp. 19–26, 2006.

[27] M. W. Raja, S. Mahanty, and R. N. Basu, "Influence of S and Ni co-doping on structure, band gap and electrochemical properties of lithium manganese oxide synthesized by soft

chemical method," *Journal of Power Sources*, vol. 192, no. 2, pp. 618–626, 2009.

[28] S. Kuppan, H. Duncan, and G. Chen, "Controlling side reactions and self-discharge in high-voltage spinel cathodes: the critical role of surface crystallographic facets," *Physical Chemistry Chemical Physics*, vol. 17, no. 39, pp. 26471–26481, 2015.

[29] D. Aurbach, B. Markovsky, M. D. Levi et al., "New insights into the interactions between electrode materials and electrolyte solutions for advanced nonaqueous batteries," *Journal of Power Sources*, vol. 81-82, pp. 95–111, 1999.

[30] D. Aurbach, B. Markovsky, G. Salitra et al., "Review on electrode-electrolyte solution interactions, related to cathode materials for Li-ion batteries," *Journal of Power Sources*, vol. 165, no. 2, pp. 491–499, 2007.

[31] K. T. Lee, S. Jeong, and J. Cho, "Roles of surface chemistry on safety and electrochemistry in lithium ion batteries," *Accounts of Chemical Research*, vol. 46, no. 5, pp. 1161–1170, 2013.

[32] K. Xu, "Nonaqueous liquid electrolytes for lithium-based rechargeable batteries," *Chemical Reviews*, vol. 104, no. 10, pp. 4303–4417, 2004.

[33] K. Xu, "Electrolytes and interphases in Li-ion batteries and beyond," *Chemical Reviews*, vol. 114, no. 23, pp. 11503–11618, 2014.

[34] D. Aurbach, Y. Talyosef, B. Markovsky et al., "Design of electrolyte solutions for Li and Li-ion batteries: a review," *Electrochimica Acta*, vol. 50, no. 2-3, pp. 247–254, 2004.

[35] M. Molenda, R. Dziembaj, D. Majda, and M. Dudek, "Synthesis and characterisation of sulphided lithium manganese spinels $LiMn_2O_{4-y}S_y$ prepared by sol-gel method," *Solid State Ionics*, vol. 176, no. 19–22, pp. 1705–1709, 2005.

[36] M. Bakierska, M. Molenda, and R. Dziembaj, "Optimization of sulphur content in $LiMn_2O_4$-$_y$$S_y$ spinels as cathode materials for lithium-ion batteries," *Procedia Engineering*, vol. 98, pp. 20–27, 2014.

[37] M. Molenda, M. Bakierska, D. Majda, M. Świętosławski, and R. Dziembaj, "Structural and electrochemical characterization of sulphur-doped lithium manganese spinel cathode materials for lithium ion batteries," *Solid State Ionics*, vol. 272, pp. 127–132, 2015.

[38] R. T. Jow, K. Xu, O. Borodin, and M. Ue, Eds., *Electrolytes for Lithium and Lithium-Ion Batteries*, Springer, New York, NY, USA, 2014.

[39] B. Ravdel, K. M. Abraham, R. Gitzendanner, J. DiCarlo, B. Lucht, and C. Campion, "Thermal stability of lithium-ion battery electrolytes," *Journal of Power Sources*, vol. 119–121, pp. 805–810, 2003.

[40] K. S. Gavritchev, G. A. Sharpataya, A. A. Smagin, E. N. Malyi, and V. A. Matyukha, "Calorimetric study of thermal decomposition of lithium hexafluorophosphate," *Journal of Thermal Analysis and Calorimetry*, vol. 73, no. 1, pp. 71–83, 2003.

[41] Q.-C. Zhuang, T. Wei, L.-L. Du, Y.-L. Cui, L. Fang, and S.-G. Sun, "An electrochemical impedance spectroscopic study of the electronic and ionic transport properties of spinel $LiMn_2O_4$," *The Journal of Physical Chemistry C*, vol. 114, no. 18, pp. 8614–8621, 2010.

[42] G. Schmid, Ed., *Nanoparticles: From Theory to Application*, John Wiley & Sons, 2011.